Soft Matter

PAPER

View Article Online
View Journal | View Issue

Cite this: *Soft Matter*, 2023, **19**, 3794

Influence of the dispersity and molar mass distribution of conjugated polymers on the aggregation type and subsequent chiral expression†

Annelien Van Oosten, [a] Cynthia Verduyckt, [a] Julien De Winter, [b] Pascal Gerbaux [b] and Guy Koeckelberghs [a]*

Received 9th February 2023,
Accepted 9th May 2023

DOI: 10.1039/d3sm00163f

rsc.li/soft-matter-journal

This study aims to determine the influence of the dispersity on the aggregation of conjugated polymers and their subsequent chiral expression. Dispersity has been thoroughly investigated for industrial polymerizations, but research on conjugated polymers is lacking. Nonetheless, knowledge thereof is crucial for controlling the aggregation type (type I *versus* type II) and its influence is therefore investigated. For that purpose, a series of polymers is synthesized *via* metered initiator addition, resulting in dispersities ranging from 1.18–1.56. The lower dispersity polymers yield type II aggregates and the resulting symmetrical electronic circular dichroism (ECD) spectra while the higher dispersity polymers are predominantly type I due to the longer chains effectively acting as a seed and therefore yield asymmetrical ECD spectra. Furthermore, a monomodal and bimodal molar mass distribution of similar dispersity are compared, demonstrating that bimodal distributions show both aggregation types and therefore more disorder, leading to a decrease in chiral expression.

Introduction

Recent work has demonstrated the influence of the aggregation type on the chiral expression of conjugated polymers (CPs), and has given an overview of many parameters that can be adjusted to control the aggregation.[1] In general, factors that lead to strong π-stacking, such as high molar mass[2] and high planarity,[3] give rise to type I aggregation (herringbone like structure), while factors benefitting van der Waals interactions, *e.g.* long sidechains,[4] will yield type II aggregated polymers with interdigitated sidechains (comb like structure).[5] However, some parameters remain unexplored, of which dispersity is the most prominent. There have been indications that dispersity has an influence on the morphology and self-assembly, mainly of block copolymers,[6–12] but in-depth knowledge of the influence of all parameters is important to control the resulting aggregation type. In turn, this is crucial for further applications as the effects of type I and type II on the electronic and optical properties differ significantly. For example, as there is a stronger π-stacking and therefore shorter interlamellar distance between adjacent chains in type I, charge transfer is facilitated by a more beneficial hopping between chains. Therefore, the presence of type I aggregates benefits applications in which a good charge transfer is essential, such as organic photovoltaic devices (oPVs), thermo-electronics and organic field effect transistors (oFETs).[13–16] In type II, the longer interlamellar distance increases fluorescence as photoluminescence quenching is diminished. This aids applications in which the optical aspects are important, such as organic light emitting devices (oLEDs).[17,18] Of course, controlling the aggregation type can help finetune applications in which the chiral properties themselves are relevant, such as metamaterials.[19]

In industrial polymerizations, the influence of dispersity is already well-known, for example in the case of polystyrene. For excellent material properties, high molar mass is necessary, usually limiting the processability of the polymer. This processability can be improved by increasing the dispersity, as the lower mass chains act as plasticizers, while the outstanding material properties originating from the higher mass chains are maintained.[20–22] Nevertheless, dispersity is only scarcely investigated in CPs, even though it differs significantly between the common synthesis procedures for CPs: a (controlled) chain-growth or a step-growth polymerization. In a controlled chain-growth polymerization, very low dispersities of around 1.05–1.1 can be obtained when the appropriate initiator is employed, for

[a] *Laboratory for Polymer Synthesis, KU Leuven, Celestijnenlaan 200F, B-3001 Heverlee, Belgium. E-mail: guy.koeckelberghs@kuleuven.be*
[b] *Organic Synthesis and Mass Spectrometry Laboratory, Center of Innovation and Research in Materials and Polymers (CIRMAP) – University of Mons (UMONS), Place du Parc 23, B-7000 Mons, Belgium*

† Electronic supplementary information (ESI) available. See DOI: https://doi.org/10.1039/d3sm00163f

example in the Kumada catalyst transfer condensative polymerization (KCTCP) of 2-bromo-3-hexyl-5-magnesiumchloride thiophene with an external *o*-tolyl [bis(diphenylphosphino)propane] nickel(II)bromide.[23,24] Other controlled CTCPs of 2-bromo-3-hexyl-5-magnesiumchloride thiophene, such as the Suzuki–Miyaura CTCP[25] or the Negishi polymerization with Pd(RuPhos),[26,27] often yield higher dispersities around 1.4, although recent methods have succeeded in narrowing the dispersity.[28] Commonly, step-growth polymerizations yield a dispersity ~ 2, but this can be much higher as well. Consequently, to adequately compare their resulting polymers, full knowledge of the influence of all parameters, including dispersity, is necessary.

In controlled polymerizations, there are a multitude of ways to vary and therefore study dispersity, which are generally divided into four categories.[29] The first one is the traditional blending of high and low molar mass chains as described above.[30,31] While this method is relatively straightforward and easily applicable to any polymer, it requires the synthesis and purification of multiple polymers and often yields a multimodal distribution, which can be undesirable for some applications. The second method is tailored catalyst concentration, in which the catalyst concentration is often extremely low (ppm range).[12,32] This can lead to several drawbacks, such as higher than intended molar mass and low conversions. Nonetheless, this method has been successfully performed by multiple groups in atom transfer radical polymerizations (ATRP) to synthesize polymers with a dispersity between 1.06 and ~ 2.[33–35] A third way to tune the dispersity, is by addition of additional reagents which can irreversibly trap a growing polymer chain.[36–38] This can either be a nonfunctional monomer, other polymer chains or terminating agents often also denoted as chain-stoppers or chain-transfer agents.[39] In many cases, addition of these agents leads to lower end-group fidelity and the formation of more advanced macromolecular structures such as block copolymers is not possible in a one-pot synthesis. The last method entails the regulation of the initiation speed, and has been demonstrated in a wide array of polymerization types such as anionic polymerization[40] and nitroxide mediated polymerization (NMP).[41] By introducing the initiator to the monomer at a selected rate, both the dispersity and the shape of the molar mass distribution can be tuned.[8] The strength of this method lies in the excellent end-group control, the high range of obtainable dispersities and the possibility to form block copolymers. Moreover, controlling the rate of initiation and propagation allows the prediction of the dispersity with high accuracy.[42] Therefore, this is the method of choice in this paper, and will be combined with KCTCP. To the best of our knowledge, this will be the first time the dispersity is varied using a CTCP of any kind in this manner.

The aim of this paper is twofold. First, a series of chiral poly(3-(3,7-(*S*)-dimethyloctyl)thiophene)s (P3DMOT) with varying dispersity is synthesized using a KCTCP in which the initiator is added to the monomer solution at variable rates. In order to do so adequately, the correct initiator and catalyst system is investigated and the reaction rate is calculated. Second, the aggregation type is determined using UV-Vis and ECD characterization. In UV-Vis, type I will give a more pronounced 0–0 transition around 635 nm due to the stronger π-stacking, *versus* a weak transition at 615 nm for a type II aggregate of P3DMOT.[43] In ECD, two neighbouring chromophores which have an angular momentum between them, will yield two similar but opposite signals, giving rise to a bisignate Cotton effect as a result of the helicity in the exciton coupling.[44,45] Recently, it has been determined that the difference in signal between both types is very pronounced as the long range interactions in type I aggregates yield an additional monosignate Cotton effect, leading to an asymmetrical spectrum.[1] Additionally, the zero-crossing occurs at higher wavelength since the polymers have an increased planarity and the zero-crossing is directly related to the absorption spectrum, which is more redshifted for type I. Therefore, the combination of both techniques provides a straightforward elucidation of the aggregation type in solution, which is an uncommon feature in other techniques. The knowledge of the influence of the dispersity on the aggregation type, and how to control this dispersity in a new manner for CTCP, will contribute to the general comparison of CPs and improvement of their properties for various applications.

Results and discussion

Four CPs with increasing dispersity are synthesized *via* KCTCP. This polymerization method is commonly known to yield low dispersities (<1.2) for poly(3-alkylthiophene)s as it is a chain-growth polymerization with a fast initiation step. Additionally, the degree of polymerization (DP) can be predicted by the initial monomer to initiator ratio, and the end groups are well controlled.[46–48] To get a range of polymers with increasing dispersity, the rate of initiation is artificially lowered by slowly adding the initiator to the active monomer using an automated syringe pump containing an initiator solution (see Scheme 1). To do so, two factors are important: solubility of the initiator and the total polymerization time. Common nickel (+II) initiators, such as [1,3-bis(diphenylphosphino)propane] dichloronickel(II) ($Ni(dppp)Cl_2$) or [1,3-bis(diphenylphosphino)ethane] dichloronickel(II) ($Ni(dppe)Cl_2$) are insoluble in THF. If this dispersion would be employed, the initiator would not be homogeneously distributed and fluctuations will occur. This can lead to both an asymmetrical molar mass distribution as the addition of initiator is not constant over time, and to deviations from the predicted average molar mass as some initiator might not be added due to sedimentation. However, to enable a concrete comparison to previous literature, external soluble initiators must be avoided as they influence the overall aggregation behavior.[49] Therefore, it is opted to oligomerize (~ 4 monomer units) a nickel (+II) salt to dissolve the catalyst and utilize this initiator solution for further polymerization (see Scheme 1). This is possible due to the controlled character of the polymerization, in which every polymer chain remains reactive as a result of the oxidative resting state of the nickel until purposeful termination.[50] In the initiation step, two monomer units are subsequently coupled by a tail-to-tail coupling as a result of two transmetallation steps in the beginning of the polymerization

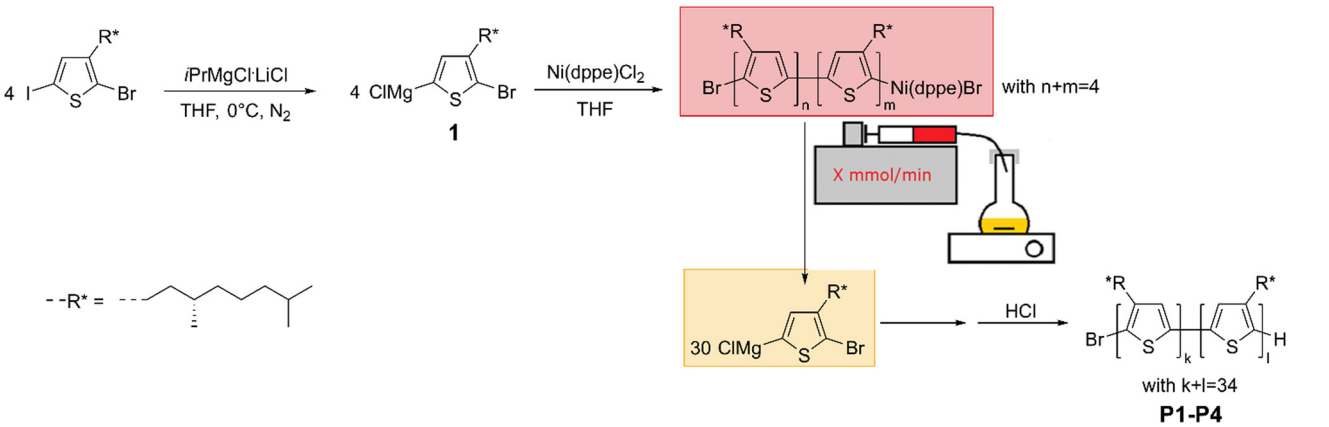

Scheme 1 Schematic representation of the polymerization reaction of **P1-P4**. The soluble initiator (red) is slowly added to the active monomer (yellow) at a rate dependent on the desired dispersity.

mechanism.[48,51] The influence of this tail-to-tail coupling is minimal, especially compared to other types of couplings or external initiators.[27] Next, the total polymerization time must be known to determine the different rates of initiator addition, as all initiator should be added to the monomer solution before the polymerization finishes to not have an excess of unreacted initiator, and to have an accurate estimation of the DP according to DP = $[monomer]_0/[initiator]$. As the rate determining step of Ni(dppp)Cl_2 is the transmetallation step (TM), the polymerization rate of Ni(dppp)Cl_2 is dependent on the monomer concentration at that moment and will therefore decline in function of conversion.[50] To ensure an equal distribution of the molar mass, it is necessary to add the initiator at a rate linearly proportional to the rate of monomer reaction. Therefore, the addition rate should exponentially decrease over time, which is experimentally unpractical. In contrast, the rate determining step of Ni(dppe)Cl_2 is the reductive elimination (RE) and is therefore monomer concentration independent and linear in function of conversion.[52] As this enables the possibility of a constant addition rate, Ni(dppe)Cl_2 was selected as the optimal pre-initiator. Note that the propagation reaction rate is catalyst dependent, so other Ni(dppe) systems such as an external aryl Ni(dppe)Br could be used in the future under similar conditions.

To determine the total reaction time, the polymerization rate constant (k_p) was determined by plotting the conversion (p) in function of reaction time (t; see Fig. 1, right). Ni(dppe) as catalyst after propagation of 4 monomer units (further referred to as 'initiator') is employed, similarly to the dispersity experiment to give an accurate indication, and to avoid deviations because of a different initiation step. Trimethoxybenzene (TMOB) is added to the monomer solution as an internal standard to calculate the unreacted amount of monomer ($n_{m,t}$) compared to the initial amount of monomer ($n_{m,0}$). Starting at time 0 (just before addition of the initiator), an aliquot of the polymerization mixture is removed every ~15 seconds, and analyzed with size exclusion chromatography (SEC) to determine the conversion (see Fig. 1, left). The conversion can be related to k_p *via* eqn (1), where $n_{m,0}$ is the

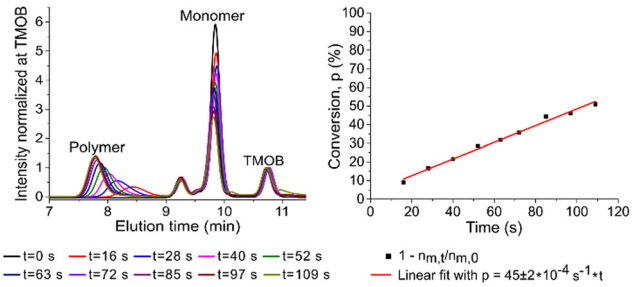

Fig. 1 Overview of the SEC chromatogram (left) normalized at the TMOB peak at 10.7 min and the resulting conversions determined as 1 minus the ratio of the amount of unreacted monomer at time t ($n_{m,t}$) over the initial amount of monomer ($n_{m,0}$) with the average least square linear fit (right). From this fit, k_p can be calculated to be 0.25 ± 0.01 s^{-1}.

initial mol active monomer, $n_{initiator}$ the amount initiator in mol, and t the time in seconds. This yields a k_p of 0.25 ± 0.01 s^{-1} for the polymerization of 2-bromo-3-(3,7-(*S*)-dimethyloctyl)-5-magnesiumchloride thiophene (**1**) with Ni(dppe) as catalyst, as $n_{initiator}$ is 0.0018 mmol and $n_{m,0}$ is 0.100 mmol.

$$p = k_p \times \frac{n_{initiator}}{n_{m,0}} \times t \quad (1)$$

As the ultimate goal of this paper is to investigate the influence of dispersity on type I and type II aggregation and their corresponding ECD signal, it is important to choose the correct range of other parameters to be able to switch between both types depending on the dispersity. This mostly means a medium-low molar mass of around ~9 kg mol^{-1} (DP ~ 30 units), as this molar mass has been determined as the switching point between type I and type II.[1] Aggregation of high molar mass almost always leads to type I aggregation, while a medium-low molar mass is sensitive to other parameters employed. In case all initiator is added at time 0, the total polymerization time can be determined from eqn (1), where p is 100%, yielding a total time of 120 s. When the initiator is slowly added over time, an integral over time needs to be calculated, as the overall reaction

speeds up in function of initiator added. Derived from eqn (1), one gets:

$$n(t) = a \times t \times k_p$$
$$\int_0^t n(t)\mathrm{d}t = a \times k_p \int_0^t t\mathrm{d}t \qquad (2)$$
$$\Delta n(t) = a \times k_p \times \frac{t^2}{2}$$

where a is the rate of initiator addition and $n(t)$ the amount of monomer reacting at time t. This equation can either be used to calculate the maximum possible addition time before the polymerization finishes (set $\Delta n(t) = n_{m,0}$ and solve for t), or to calculate the amount of monomer reacted when all initiator is added. From the combination of eqn (1) and (2), a total polymerization time can be calculated based on a given addition rate a and total addition time. To get a trend of increasing dispersity, four different addition times were chosen, resulting in four polymers (see Table 1). It must be noted that for **P4**, the total addition time is slightly longer than the calculated polymerization time. As it was observed in previous experiments that termination of some initiator oligomers could not be fully prohibited, the addition time of the polymer with the highest aimed dispersity was increased by ~10% compared to the maximum polymerization time to allow for the largest possible dispersity. Should the polymerization be finished before all initiator is added, the molar mass would have increased, which is clearly not the case. Before characterization, all polymers are purified by a Soxhlet extraction with *iso*propylalcohol to remove any unreacted initiator present. Afterwards, the synthesized polymers are characterized by SEC, ^{1}H-NMR and matrix-assisted laser desorption/ionization time-of-flight (MALDI-ToF) for the determination of their mass parameters (number average molar mass ($\bar{M}_n$), weight average molar mass ($\bar{M}_w$) and dispersity ($Đ$)) as well as the nature of the end-groups (see ESI† and Table 1). Note that this approach provides for the first time conjugated polymers of which both molar mass and dispersity can be independently varied. Compared to some industrially synthesized polymers, the dispersity is still rather limited as a result of the medium-low molar mass. A broader distribution would in this case also lead to an increase in molar mass, which should be avoided as the polymers would always aggregate according to type I at high molar mass.

A plot of the actual SEC chromatograms demonstrates that the molar mass distribution broadens (see Fig. 2). The different chromatograms are normalized by their area, meaning that the total area of each graph is identical, which leads to a decrease

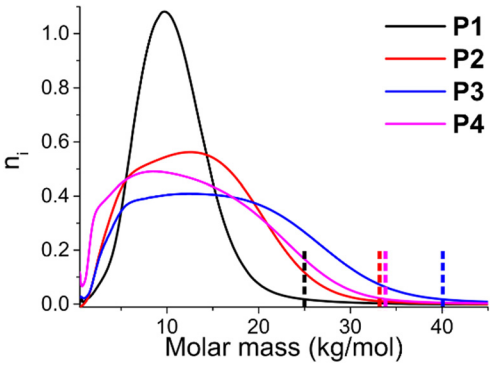

Fig. 2 Overview of the SEC chromatograms of **P1-P4**. The graphs are recalculated towards their molar mass according to the calibration curve (based on polystyrene standards in THF). The dotted lines represent the maximum molar mass where the elution curves reach zero. Furthermore, they are area corrected, so that each polymer exhibits the same total integration value of the curve, and plotted in function of n_i, the relative amount of chains of that molar mass.

in height when the dispersity broadens. Due to the relatively low molar mass, it is not possible to create fully symmetrical molar mass distributions, as there is a lower limit, and the distributions are slightly skewed towards higher molar mass. The sudden decrease at very low molar mass is a result of the Soxhlet purification in which these short oligomers are removed. Overall, it can be observed that the molar mass distributions become broader with increasing dispersity, and that the maximum molar mass present at the right limit of the molar mass distribution increases substantially, from 25 kg mol^{-1} for **P1** to 40 kg mol^{-1} to **P3** (taken as the point where the SEC elution curve reaches zero, see dotted lined in Fig. 2). The highest molar mass is ~33 kg mol^{-1} for **P4** even though it has the highest dispersity, as the $\bar{M}_n$ of this polymer is also the lowest overall.

To induce aggregation, the polymers are dissolved in chloroform ($CHCl_3$) and the non-solvent methanol (MeOH) is added stepwise (see ESI† for full details). The polymers slowly transition from a random coil conformation to aggregated stacks, in which either π-stacking (type I) or van der Waals interactions (type II) dominate. ECD measurements are commonly employed in chiral CPs and here utilized to impartially and straightforwardly determine the correct aggregation type of the solution.[53–57] Specifically, type I aggregation has a more effective long range interaction due to closer interlamellar distances and stronger π-stacking, leading to an additional monosignate Cotton effect. Contrarily, a symmetrical bisignate Cotton effect is expected in type II as the interactions are mostly governed by the

Table 1 Overview of the polymerization rate specifications and resulting molar mass parameters obtained by SEC analysis for **P1-P4**. The polymers are measured in THF against polystyrene standards

	Addition time	Addition rate	Total time of polymerization	$\bar{M}_n$ (kg mol^{-1})	$\bar{M}_w$ (kg mol^{-1})	$Đ$
P1	1 min	0.01 mmol min^{-1}	150 s	9.3	10.9	1.18
P2	2 min	0.005 mmol min^{-1}	180 s	9.8	13.5	1.37
P3	3 min	0.00333 mmol min^{-1}	210 s	11.3	16.7	1.48
P4	5 min	0.002 mmol min^{-1}	268 s	8.4	13.0	1.56

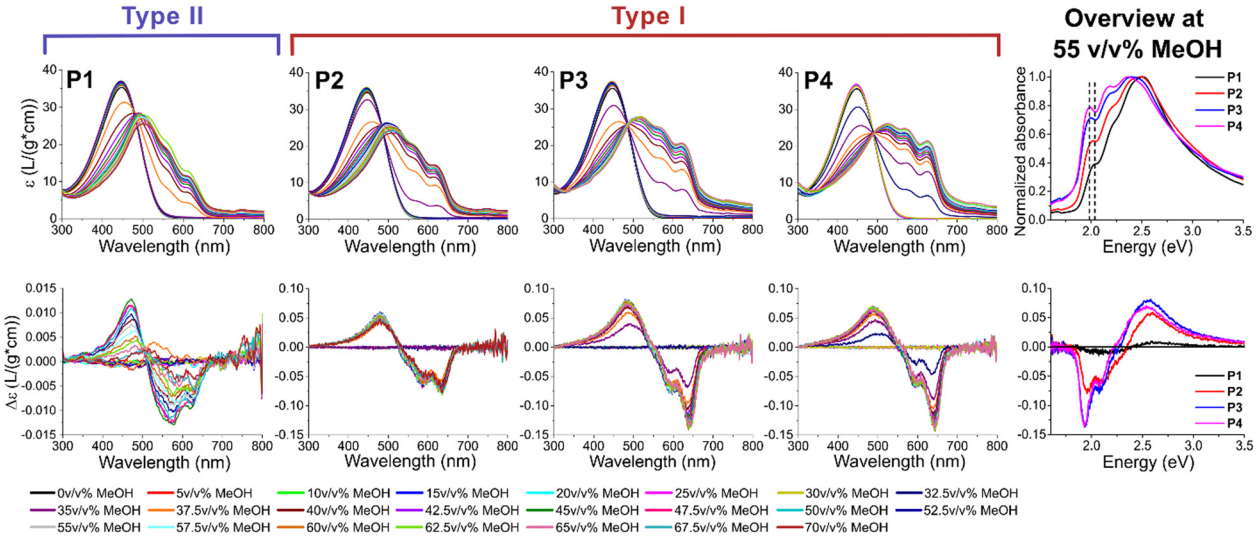

Fig. 3 The UV-vis (top) and ECD spectra (bottom) of the solvatochromism experiments for **P1-P4**. Note that the ECD spectrum for **P1** has a different *y*-axis and is smoothed with the adjacent-averaging method for clarity. On the right, an overview of all polymers at 55 v/v% MeOH is presented to clarify the bathochromic shift (dotted line) and change in ECD spectrum from low to high dispersity.

sidechains.[1] This technique is less complicated and more readily available than other common techniques to determine the aggregation type, such as X-ray diffraction (XRD) or selected area electronic diffraction (SAED). Furthermore, ECD has the advantage that the process of aggregation can be investigated as not only the final state (thin film) is measured, and that only short range interactions are required, while other techniques require (high) crystallinity. Additionally, the onset of aggregation is determined by UV-Vis spectroscopy by the presence of a bathochromic shift of the π–π* transition and the appearance of finestructure. The bathochromic shift is the result of planarization, increasing the effective conjugation length upon aggregation. This finestructure is a result of different vibronic transitions, of which the 0–0 transition at ∼635 nm for type I and ∼615 nm for type II is mostly of interest for determining the amount of π-stacking.[58] This transition clearly shifts towards higher wavelength (lower energy levels) and becomes more pronounced with increasing dispersity (see Fig. 3, right) with the transition at the highest wavelength (630 nm or 1.97 eV) present in **P4**. The reason for this bathochromic shift upon transition from type I to type II is directly related to the driving forces of their aggregation: π–π stacking and van der Waals forces, respectively. The stronger π–π stacking in type I, and resulting closer interlamellar distance between neighboring polymer chains, leads to a stronger planarization upon aggregation. This planarization in turn leads to a more efficient delocalization of the electrons, effectively decreasing their energy transition levels. Analyzing the ECD chromatograms, a clear trend is observed in function of dispersity (see Fig. 3). At low dispersity (**P1**), the polymer initially forms type II upon aggregation, while type I is also formed at high MeOH percentages. This can be concluded from a change in sign of the spectrum after 40 v/v% MeOH. Nonetheless, the spectrum remains relatively symmetrical, and the zero-crossing occurs at higher energy (lower wavelength) compared to the other polymers. **P2** can be considered an intermediate aggregation state with both type I and II present, both from the intermediate zero-crossing, the relatively low amount of π-stacking and the fairly symmetrical ECD spectrum, even though the monosignate peak is already clearly visible. This monosignate peak is the result of long range order, which is more prevalent in type I aggregates, as their stronger π–π stacking leads to a shorter interlamellar distance. At the highest dispersity (**P3** and **P4**), type I prevails distinctly. When comparing the ECD spectra after full aggregation (55 v/v% MeOH) of **P1-P4**, the increase of the monosignate contribution at 635 nm (1.95 eV) and the zero-crossing at progressively higher wavelength (lower energy) in function of increasing dispersity is clear (see Fig. 3, right). For **P3** and **P4**, the ECD spectra are almost identical, even though the amount of π-stacking still increases for **P4** according to the UV-Vis spectra. This is particularly interesting as the $\bar{M}_n$ and $\bar{M}_w$ are slightly lower for **P4** than for **P3**, indicating that the formation of type I is effectively derived from the higher dispersity and not a result of the higher mass of **P3**. The measurements are repeated to confirm their reproducibility (see ESI†).

To determine the influence of the low *versus* high molar mass chains on the overall aggregation behavior, two mixtures were prepared of two different low dispersity polymers (low molar mass **P5** and high molar mass **P6**). The first mixture (**M1**) had the same mass of both polymers, while in the second mixture (**M2**) both polymers were present in an equimolar amount (see Table 2; full characterization can be found in the ESI†). Although the average molar masses of **M1** and **M2** diverge due to the varying amounts of low molar mass **P5** and high molar mass **P6**, both are in range of **P3** and **P4** of the previous experiments. Similarly, the overall dispersity of the mixtures is in range of **P3** and **P4**, even though the actual

Table 2 Overview of the molar mass parameters obtained by SEC analysis for the low molar mass **P5** and high molar mass **P6**, together with their resulting mixtures **M1-M2**

	Molar ratio of **P5**	Molar ratio of **P6**	$\bar{M}_n$ (kg mol^{-1})	$\bar{M}_w$ (kg mol^{-1})	$Đ$
P5	100	0	5.2	6.0	1.17
P6	0	100	15.0	16.9	1.15
M1	73	27	7.6	11.4	1.49
M2	50	50	10.3	14.7	1.43

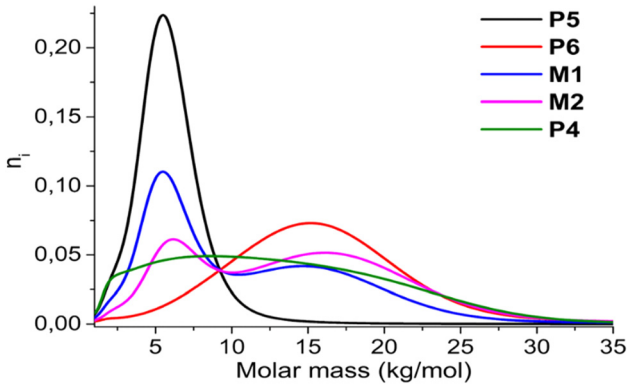

Fig. 4 Overview of the SEC chromatograms of **P5-P6** and the mixtures **M1-M2**, overall compared to **P4**. The graphs are recalculated towards their molar mass according to the calibration curve (based on polystyrene standards in THF). Furthermore, they are area corrected, so that each polymer exhibits the same total integration value of the curve, and plotted in function of n_i, the relative amount of chains of that molar mass.

molar mass distribution is different (see Fig. 4). In the mixtures, an increased amount of lower and higher molar mass chains is present, with a gap between them due to the absence of intermediate length chains. This gap enables separate comparison of the short and long chains, as both are known to exhibit different aggregation behavior, and is therefore a means to determine possible interactions between chains of different lengths.[2] Longer chains typically aggregate at lower amounts of non-solvent, and starting at ~10 kg mol^{-1},[59] they usually chain fold, while tie crystals can occur at a molar mass higher than 19 kg mol^{-1}.[60] On the other hand, shorter chains have recently been shown to aggregate in a two-step process, where the first step forms sheet-like structures with interdigitated sidechains without further π-stacking (pre-aggregation).[1] Mixing both without a smooth transition enables the determination of the type of chain/aggregate that takes the lead as the seed of aggregation, while also determining the effect of a bimodal *versus* monomodal molar mass distribution.

To adequately ascertain which events originate from the short or long polymer chains, **P5** and **P6** are assessed first to reveal their individual effect (see Fig. 5, left). As already described in previous literature, the low molar mass polymers typically aggregate according to type II, while high molar mass polymers have a tendency to aggregate according to type I.[2] When measuring **P5** and **P6** with UV-Vis spectroscopy and ECD, analogous to the previous experiment, it is indeed confirmed that **P5** displays the typical symmetrical ECD spectra for type II, while **P6** has an additional monosignate Cotton effect due to the long range interactions in type I. Whereas the ECD signal of **P6** is almost identical to those of **P3** and **P4**, the mixtures **M1** and **M2** show a much more symmetrical and smaller ECD effect, indicating that both type I and II are present. This is also clearly observed in the initial aggregation phase of **M2**, which has an opposite sign and is indicative of type II. This is very surprising, as it is generally believed that high molar mass (type I) chains aggregate first since their solubility is lower. The initial formation of type II could be a result of the pre-aggregation formation of sheet-like structures, which already

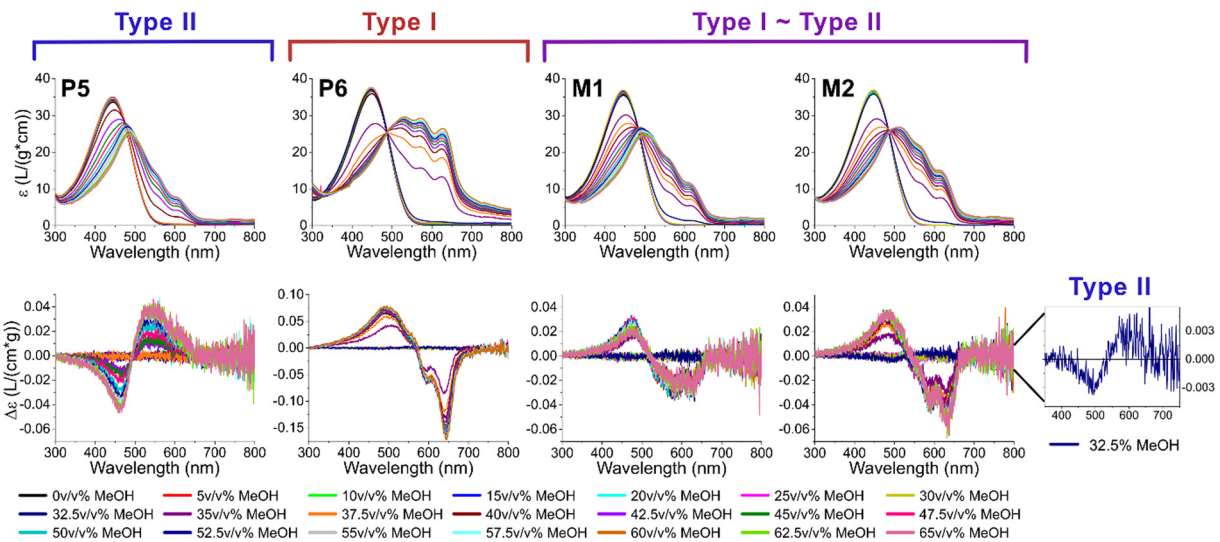

Fig. 5 The UV-vis (top) and ECD spectra (bottom) of the solvatochromism experiments for **P5-P6** and their mixtures **M1-M2**. Note that *y*-axis of the ECD graph of **P6** is on a different scale from the others. On the right, a zoomed inset of **M2** at the onset of aggregation (32.5 v/v% MeOH) shows that initially type II aggregates are formed.

occurs at 25–30 v/v% MeOH.[1] Nonetheless, this "seed" is not continued as afterwards the sign switches and type I is formed, indicating that both types are present in the mixture. If the short and long chains would aggregate completely independently, the resulting ECD spectra of the mixtures should be a weighted average of the individual polymers, which is not the case (see ESI†). Overall, a similar shape can be observed, but the intensity of the signal is about halved, and more in range of what is typically observed for type II, or polymers who are on edge between both types. We therefore hypothesize that the presence of type II aggregates disrupts the long range order of type I aggregates, leading to a less pronounced monosignate effect. When comparing **M1** and **M2**, the latter shows a more pronounced monosignate peak at 635 nm, presumably due to the higher overall molar mass.

By comparing the mixtures **M1** and **M2** to **P3** and **P4**, which are all similar in molar mass and dispersity, but differ in the shape of their molar mass distribution, a mechanism of the formation of type I aggregates in high dispersity polymers can be proposed. In general, aggregate formation occurs readily when there is little difference between the aggregating units. In polymers, this translates to the necessity of similar molar mass chains to form the most optimal stacks. If a polymer is longer than its neighbor, the remainder of the chain has no possibilities to form π-stacks and will form dangling ends which are less favorable due to a larger free surface energy. If a polymer is shorter than its neighbor, not all possible π-stacks are utilized, which is enthalpically less favorable. Herein, the distinction between monomodal (**P3** and **P4**) and bimodal (**M1** and **M2**) becomes relevant. In the monomodal distribution, on the one hand, a continuous increase/decrease in chain length between all polymer chains is present. Therefore, the high molar mass polymers aggregate first according to type I, and on this seed, increasingly shorter chains can gradually stack, while keeping the initial aggregation type (see Fig. 6). The short polymer chains can form sheets with interdigitating sidechains, but they are unlikely to form a type II seed. As there is only a small amount of short chains present, the sheets are more inclined to reversibly dissociate and propagate on the type I seed than stacking multiple sheets together to form a nucleation point as their aggregation point occurs slowly and at higher methanol percentages.[1] In the bimodal distribution, on the other hand, there is a discrepancy between the lower and higher molar mass fraction with a larger amount of both lower and higher molar mass chains present compared to **P3** and **P4**. Therefore, they aggregate relatively independently of each other. Consequently, two different seeds are formed, resulting in the presence of two aggregation types. The presence of both aggregation types leads to more overall disorder and disruption of the long range π–π stacking. Correspondingly, the chiral expression is lower than expected.

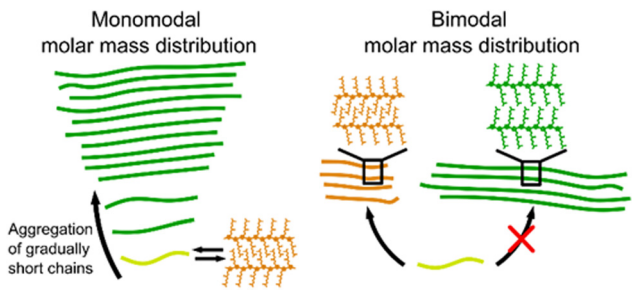

Fig. 6 Schematic representation of the differences in aggregation between polymers with a monomodal molar mass distribution (type I aggregates) *versus* a bimodal molar mass distribution (both type I and II aggregates present).

Conclusions

For the first time, a combination of metered initiation addition and KCTCP is successfully employed to vary the dispersity in a controlled manner. Ni(dppe)Cl_2 is selected as a suitable pre-initiator due to its rate invariability towards conversion, making linear initiator addition possible. The polymerization rate constant of a Ni(dppe) catalyst with a 2-bromo-3-(3,7-(*S*)-dimethyloctyl)-5-magnesiumchloride thiophene monomer is calculated at 0.25 ± 0.01 s^{-1}. Four polymers are synthesized with a total initiator addition time between 1 and 5 min, yielding polymers with dispersities ranging from 1.18 to 1.56. Solutions of these polymers are aggregated due to non-solvent addition, and their resulting aggregation type is characterized with UV-Vis and ECD spectroscopy. It is determined that polymers with low dispersity tend to aggregate according to type II with the resulting symmetric ECD spectra, while high dispersity polymers form type I aggregates and the corresponding asymmetric ECD spectra. By comparing these monomodal distributions with a mixture of a short and long polymer solution with a similar molar mass and dispersity, an aggregation mechanism is proposed. The mixtures show clear presence of both aggregation types, originating from both individual polymers, leading to a low monosignate Cotton effect in ECD due to disruption of the long range type I aggregates. In contrast, monomodal polymers with a similar dispersity predominantly aggregate according to type I, as the high molar mass chains aggregate first and act as a seed, and shorter polymer chains can adhere continuously to this seed. In conclusion, this paper demonstrates a new manner to control the dispersity in conjugated polymers, while simultaneously determining the influence of this dispersity and the shape of the molar mass distribution on the aggregation behavior and chiral expression. Given the fact that the dispersity of conjugated polymers can vary significantly as a result of different polymerization techniques, we have identified the dispersity as an important but yet overlooked parameter for the properties of conjugated polymers.

Author contributions

All authors have given approval to the final version of the manuscript. All authors significantly contributed to this research. A. Van Oosten and C. Verduyckt were the main contributors to the investigation, the methodology and the validation. A. Van Oosten

conducted the visualisation and writing of the original draft. P. Gerbaux and J. De Winter were responsible for the formal analysis and investigation of the MALDI-ToF data. G. Koeckelberghs is responsible for conceptualization, funding acquisition, project administration and supervision. All authors contributed evenly to the review and editing of writing this manuscript.

Conflicts of interest

There are no conflicts to declare.

Acknowledgements

This research was funded by Onderzoeksfonds KU Leuven/ Research Fund KU Leuven.

Notes and references

1 A. Van Oosten, K. Aerts, Y. de Coene, J. De Winter, P. Gerbaux, T. Verbiest and G. Koeckelberghs, submitted.
2 Y. Guo, L. Wang, Y. Han, Y. Geng and Z. Su, *Polym. Chem.*, 2014, **5**, 1938–1944.
3 S. V. Meille, V. Romita, T. Caronna, A. J. Lovinger, M. Catellani and L. Belobrzeckaja, *Macromolecules*, 1997, **30**, 7898–7905.
4 T. J. Prosa, M. J. Winokur and R. D. McCullough, *Macromolecules*, 1996, **29**, 3654–3656.
5 R. Noriega, J. Rivnay, K. Vandewal, F. P. V. Koch, N. Stingelin, P. Smith, M. F. Toney and A. Salleo, *Nat. Mater.*, 2013, **12**, 1038–1044.
6 N. A. Lynd, A. J. Meuler and M. A. Hillmyer, *Prog. Polym. Sci.*, 2008, **33**, 875–893.
7 N. A. Lynd and M. A. Hillmyer, *Macromolecules*, 2005, **38**, 8803–8810.
8 T. M. Beardsley and M. W. Matsen, *Eur. Phys. J. E: Soft Matter Biol. Phys.*, 2008, **27**, 323–333.
9 D. T. Gentekos, J. Jia, E. S. Tirado, K. P. Barteau, D. M. Smilgies, R. A. Distasio and B. P. Fors, *J. Am. Chem. Soc.*, 2018, **140**, 4639–4648.
10 B. Oschmann, J. Lawrence, M. W. Schulze, J. M. Ren, A. Anastasaki, Y. Luo, M. D. Nothling, C. W. Pester, K. T. Delaney, L. A. Connal, A. J. McGrath, P. G. Clark, C. M. Bates and C. J. Hawker, *ACS Macro Lett.*, 2017, **6**, 668–673.
11 J. M. Widin, A. K. Schmitt, A. L. Schmitt, K. Im and M. K. Mahanthappa, *J. Am. Chem. Soc.*, 2012, **134**, 3834–3844.
12 J. Listak, W. Jakubowski, L. Mueller, A. Plichta, K. Matyjaszewski and M. R. Bockstaller, *Macromolecules*, 2008, **41**, 5919–5927.
13 Y. Wang, H. Cui, M. Zhu, F. Qiu, J. Peng and Z. Lin, *Macromolecules*, 2017, **50**, 9674–9682.
14 P. E. Keivanidis, J. I. Khan, L. Katzenmeier, Z. Kan, S. Limbu, M. Constantinou, E. Lariou, G. Constantinides, S. C. Hayes, J. S. Kim and F. Laquai, *J. Phys. Chem. C*, 2018, **122**, 29141–29149.
15 K. S. Ahn, H. Jo, J. B. Kim, I. Seo, H. H. Lee and D. R. Lee, *ACS Appl. Mater. Interfaces*, 2020, **12**, 1142–1150.
16 C. Poelking and D. Andrienko, *Macromolecules*, 2013, **46**, 8941–8956.
17 Z. L. Gong, X. Zhu, Z. Zhou, S. W. Zhang, D. Yang, B. Zhao, Y. P. Zhang, J. Deng, Y. Cheng, Y. X. Zheng, S. Q. Zang, H. Kuang, P. Duan, M. Yuan, C. F. Chen, Y. S. Zhao, Y. W. Zhong, B. Z. Tang and M. Liu, *Sci. China: Chem.*, 2021, **64**, 2060–2104.
18 T. Kobayashi, K. Kinoshita, A. Niwa, T. Nagase and H. Naito, *Nanoscale Res. Lett.*, 2017, **12**, 268.
19 B. Nowacki, H. Oh, C. Zanlorenzi, H. Jee, A. Baev, P. N. Prasad and L. Akcelrud, *Macromolecules*, 2013, **46**, 7158–7165.
20 D. Nichetti and I. Manas-Zloczower, *Polym. Eng. Sci.*, 1999, **39**, 887–895.
21 M. Nadgorny, D. T. Gentekos, Z. Xiao, S. P. Singleton, B. P. Fors and L. A. Connal, *Macromol. Rapid Commun.*, 2017, **38**, 1–5.
22 X. Ye and T. Sridhar, *Macromolecules*, 2005, **38**, 3442–3449.
23 A. Smeets, P. Willot, J. De Winter, P. Gerbaux, T. Verbiest and G. Koeckelberghs, *Macromolecules*, 2011, **44**, 6017–6025.
24 A. Smeets, K. Van Den Bergh, J. De Winter, P. Gerbaux, T. Verbiest and G. Koeckelberghs, *Macromolecules*, 2009, **42**, 7638–7641.
25 T. Yokozawa, R. Suzuki, M. Nojima, Y. Ohta and A. Yokoyama, *Macromol. Rapid Commun.*, 2011, **32**, 801–806.
26 P. Willot, J. Steverlynck, D. Moerman, P. Leclère, R. Lazzaroni and G. Koeckelberghs, *Polym. Chem.*, 2013, **4**, 2662–2671.
27 L. Verheyen, J. De Winter, P. Gerbaux and G. Koeckelberghs, *Macromolecules*, 2019, **52**, 8587–8595.
28 K. Kosaka, T. Uchida, K. Mikami, Y. Ohta and T. Yokozawa, *Macromolecules*, 2018, **51**, 364–369.
29 R. Whitfield, N. P. Truong, D. Messmer, K. Parkatzidis, M. Rolland and A. Anastasaki, *Chem. Sci.*, 2019, **10**, 8724–8734.
30 N. Corrigan, A. Almasri, W. Taillades, J. Xu and C. Boyer, *Macromolecules*, 2017, **50**, 8438–8448.
31 R. Whitfield, N. P. Truong and A. Anastasaki, *Angew. Chem., Int. Ed.*, 2021, **60**, 19383–19388.
32 R. Whitfield, K. Parkatzidis, M. Rolland, N. P. Truong and A. Anastasaki, *Angew. Chem., Int. Ed.*, 2019, **58**, 13323–13328.
33 M. Rolland, N. P. Truong, R. Whitfield and A. Anastasaki, *ACS Macro Lett.*, 2020, **9**, 459–463.
34 A. Plichta, M. Zhong, W. Li, A. M. Elsen and K. Matyjaszewski, *Macromol. Chem. Phys.*, 2012, **213**, 2659–2668.
35 Z. Wang, J. Yan, T. Liu, Q. Wei, S. Li, M. Olszewski, J. Wu, J. Sobieski, M. Fantin, M. R. Bockstaller and K. Matyjaszewski, *ACS Macro Lett.*, 2019, **8**, 859–864.
36 K. Parkatzidis, N. P. Truong, M. N. Antonopoulou, R. Whitfield, D. Konkolewicz and A. Anastasaki, *Polym. Chem.*, 2020, **11**, 4968–4972.
37 S. I. Rosenbloom, R. J. Sifri and B. P. Fors, *Polym. Chem.*, 2021, **12**, 5910–5915.

38 V. Yadav, N. Hashmi, W. Ding, T. H. Li, M. K. Mahanthappa, J. C. Conrad and M. L. Robertson, *Polym. Chem.*, 2018, **9**, 4332–4342.
39 X. Liu, C. G. Wang and A. Goto, *Angew. Chem., Int. Ed.*, 2019, **58**, 5598–5603.
40 V. Kottisch, D. T. Gentekos and B. P. Fors, *ACS Macro Lett.*, 2016, **5**, 796–800.
41 D. T. Gentekos, L. N. Dupuis and B. P. Fors, *J. Am. Chem. Soc.*, 2016, **138**, 1848–1851.
42 S. Domanskyi, D. T. Gentekos, V. Privman and B. P. Fors, *Polym. Chem.*, 2020, **11**, 326–336.
43 P. J. Brown, D. S. Thomas, A. Köhler, J. S. Wilson, J. S. Kim, C. M. Ramsdale, H. Sirringhaus and R. H. Friend, *Phys. Rev. B: Condens. Matter Mater. Phys.*, 2003, **67**, 1–16.
44 E. R. Lermo, B. M. W. Langeveld-voss, R. A. J. Janssen and E. W. Meijer, *Chem. Commun.*, 1999, 791–792.
45 B. M. W. Langeveld-Voss, D. Beljonne, Z. Shuai, R. A. J. Janssen, S. C. J. Meskers, E. W. Meijer and J. L. Brédas, *Adv. Mater.*, 1998, **10**, 1343–1348.
46 T. Yokozawa and A. Yokoyama, *Polym. J.*, 2004, **36**, 65–83.
47 A. Yokoyama, R. Miyakoshi and T. Yokozawa, *Macromolecules*, 2004, **37**, 1169–1171.
48 M. C. Iovu, E. E. Sheina, R. R. Gil and R. D. McCullough, *Macromolecules*, 2005, **38**, 8649–8656.
49 M. P. Van Den Eede, A. Bedi, J. Delabie, J. De Winter, P. Gerbaux and G. Koeckelberghs, *Polym. Chem.*, 2017, **8**, 5666–5672.
50 E. L. Lanni and A. J. McNeil, *Macromolecules*, 2010, **43**, 8039–8044.
51 R. Miyakoshi, A. Yokoyama and T. Yokozawa, *J. Am. Chem. Soc.*, 2005, **127**, 17542–17547.
52 E. L. Lanni and A. J. McNeil, *J. Am. Chem. Soc.*, 2009, **131**, 16573–16579.
53 A. R. A. Palmans and E. W. Meijer, *Angew. Chem., Int. Ed.*, 2007, **46**, 8948–8968.
54 K. Wang and Y. Xiao, *Chirality*, 2021, **33**, 424–446.
55 T. Yamamoto, *Macromol. Rapid Commun.*, 2002, **23**, 583–606.
56 T. Yamamoto, *Bull. Chem. Soc. Jpn.*, 2010, **83**, 431–455.
57 Z.-B. Zhang, M. Fujiki, M. Motonaga, H. Nakashima, K. Torimatsu and H.-Z. Tang, *Macromolecules*, 2002, **35**, 941–944.
58 Y. Qu, Q. Su, S. Li, G. Lu, X. Zhou, J. Zhang, Z. Chen and X. Yang, *ACS Macro Lett.*, 2012, **1**, 1274–1278.
59 J. Liu, M. Arif, J. Zou, S. I. Khondaker and L. Zhai, *Macromolecules*, 2009, **42**, 9390–9393.
60 M. Brinkmann and P. Rannou, *Macromolecules*, 2009, **42**, 1125–1130.

